13th ewtec 2019
Proceedings of the 13th European Wave and Tidal Energy Conference 1-6 Sept 2019, Naples, Italy

High resolution large eddy simulation for tidal site turbulence characterisation

Philippe Mercier, Mikaël Grondeau, Sylvain Guillou, Jérôme Thiébot, and Emmanuel Poizot

***Abstract*—The assessment of turbulence characteristics at a tidal power site is a prerequisite for near future installation of industrial tidal turbine farms. Computing costs still penalize unsteady numerical simulations of tidal flows. The lattice Boltzmann method associated with large eddy simulation is particularly adequate to simulate flows on such large and complex domains. A simulation involving a real bathymetry is conducted. First results are promising, as the model results fit well the turbulence characteristics measured by ADCP near the seabed. In this article, we show the possible contribution of the model in understanding the turbulent processes in the Raz Blanchard. Such results may have great implications for tidal site characterization.**

***Index Terms*—Computational fluid dynamics, large eddy simulation, lattice Boltzmann method, seabed morphology, tidal power, turbulence**

I. Introduction

The industrial development of tidal stream power in a near future calls for a deep understanding of environmental conditions and flow characteristics. The extractable power on promising sites is assessed through regional numerical flow simulations [1], [2]. Simplified models of turbines such as actuator disc [3] or models of turbine farms such as enhanced bottom friction [4] may be integrated in these simulations to help optimize tidal turbine positioning [5] and assess the impact of tidal turbine farms on environmental flows [6]. Comparisons with on-site measurements [7] demonstrate the need for innovative approach to simulate and characterize the turbulence at tidal stream energy sites.

Turbulence has large effects on tidal turbines [8], [9]. However, the knowledge of tidal site turbulence is not exhaustive. Despite difficulties related to the harsh environment, measurements with ADCP (Acoustic Doppler Current Profiler) or ADV (Acoustic Doppler Velocimeter) are widely used [10], [11], [12]. They provide a good understanding of the turbulence at a particular location. However, such results cannot be extrapolated over a large zone because the turbulence is spatially highly heterogeneous. Indeed, it depends on the local hydrodynamics and seabed morphology but it is also influenced by far-field effects. Numerical modelling could complete this missing information. The model should be accurate enough in time and space to allow modelling the effect of fine seabed morphology details on a vast area, which is a big challenge.

Large Eddy Simulation (LES) method [13] is suited for simulating the unsteady behavior of tidal flows and assessing the turbulence caracteristics. It may be associated with the Lattice Boltzmann Method (LBM), that numerically solves the Boltzmann equation [14]. As this approach is explicit, it allows massively parallel simulations and can thus be used to compute the flow over large domains with refined mesh.

For the present purpose, simulations of a tidal power flow at a local scale are performed, using LBM associated with LES. The numerical tool, based on the Palabos open-source C++ library for LBM, was validated with experimental data acquired in a turbulent open channel flow above macro-roughness [15]. This validation was a prerequisite to simulate turbulent flows at real tidal power sites such as the Raz Blanchard (see Figure 1). The present contribution, carried out within the THYMOTE project, consists in simulating, at a local scale, the effect of the seabed morphology on the turbulence. This method is applied to the Raz Blanchard.

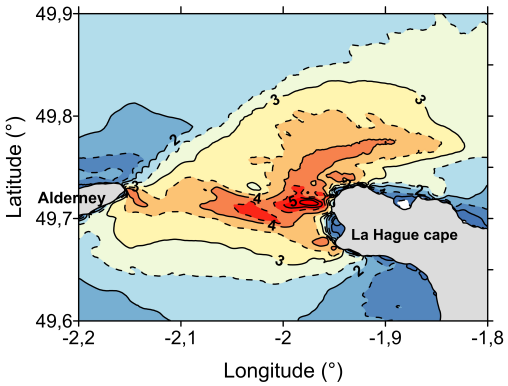

Fig. 1. Annual maximal tidal current speed in the Raz Blanchard.

II. Numerical background

The Lattice Boltzmann Method is well suited for simulation of large and complex domains such as a tidal flow over a rough seabed. This section is a reminder of the main insight of this method. A more complete description can be found in [15].

ID number: 1666. Tidal resource characterization.
This work benefits from a French State grant managed by the National Research Angency under the Investments for the Future program bearing the reference ANR-10-IEED-0006-11, as well as computational means funded by the Manche Council and those of the CRIANN
P. Mercier, M. Grondeau, S. Guillou, J. Thiébot and E. Poizot are at the French Universitary Laboratory of Applied Science of Cherbourg (LUSAC) 60 rue Max Pol Fouchet Cherbourg, 50100 France (e-mails: philippe.mercier, mikael.grondeau, sylvain.guillou, jerome.thiebot, emmanuel.poizot, @unicaen.fr).

 Copyright © European Tidal and Wave Energy Conference 2019

A. The lattice Boltzmann method

The Lattice Boltzmann Method defines a fluid as a composition of agitated molecules. It describes the flow from the individual behaviour of the molecules using a statistical description. A collision operator models the interaction between particles and allows calculating the molecule speed changes. This requires the introduction of distribution function.

The distribution function $f(\vec{x},\vec{c},t)$ quantifies the density of molecules situated at position $\vec{x}$ at time t and moving at speed $\vec{c}$. The density and the velocity are deduced from this function by an integration of the density and of the first momentum on the whole speed space (Equation 1 and Equation 2).

$$\int f(\vec{x},\vec{c},t)\vec{dc} = \rho(\vec{x},t). \tag{1}$$

$$\int f(\vec{x},\vec{c},t)\vec{c}\vec{dc} = \rho\vec{u}(\vec{x},t) \tag{2}$$

The numerical treatment of a distribution function implies its discretization with respect to its three continuous variables (position, time and velocity). Spatial discretization is performed on a Cartesian lattice of nodes spaced by a Δx length. The time discretization corresponds to the time Δt between two computation steps. The velocity space is narrowed to the velocities allowing joining a fixed number of neighbour nodes in a Δt time. The number and positions of retained neighbour nodes depend on a chosen scheme. A usual 3D scheme uses 19 nodes.

The distribution function evolution obeys to the Boltzmann equation (Equation 3), where $\vec{\nabla}$ is the classical gradient operator and Ω is the collision operator. After discretization, this equation becomes Equation 4 with i varying between 0 and 18.

$$\frac{\partial f(\vec{x},\vec{c},t)}{\partial t} + \vec{c}.\vec{\nabla}(f(\vec{x},\vec{c},t)) = \Omega(f) \tag{3}$$

$$f_i(\vec{x}+\Delta t\vec{c_i}, t+\Delta t) - f_i(\vec{x},t) = \Omega_i(\vec{x},t) \tag{4}$$

The calculation of the distribution function at time $t+\Delta t$ is then straightforward. The difficulty relies on the definition of the collision operator Ω.

The most known collision operator is the BGK operator Ω_{BGK} [16]. It is based on the principle that collisions lead distribution functions towards an equilibrium state. This equilibrium state corresponds to the Maxwell velocity distribution $f_{Maxwell}$ [17]. The BGK operator writes as follows:

$$\Omega_{BGK_i}(\vec{x},t) = -\frac{f_i(\vec{x},t) - f_i(\vec{x},t)_{Maxwell}}{\tau(\nu)} \tag{5}$$

where ν is the kinematic viscosity and $\tau(\nu)$ is a relaxation time defined as:

$$\tau(\nu) = 3\nu\frac{\Delta t}{\Delta x^2} + 0.5. \tag{6}$$

Latt [18] introduced a regularization procedure to handle high Reynolds number simulations with a good numerical stability.

B. Large eddy simulation

The domain discretization implies a loss of information on eddies smaller than the mesh resolution. A sub-grid model compensates this loss by modelling the effect of small eddies. This method is inspired by Smagorinsky work [19], and well described by Sagaut [13] for Navier-Stokes equation applications. The same principle can be adapted to LBM [14]. The Boltzmann equation is spatially filtered, and only the large-scale eddies are simulated. The sub-grid model used is the static Smagorinsky model [19], [20]. It consists of an additional viscosity ν_t named turbulent viscosity calculated from Equation 7:

$$\nu_t = (C_S\Delta x)^2|\overline{\overline{S}}| \tag{7}$$

with $\overline{\overline{S}}$ the strain-rate tensor and C_S the Smagorinsky constant, uniformly set to 0.14. This directly impacts the value of the relaxation time $\tau = \tau(\nu+\nu_t)$.

III. RAZ BLANCHARD

The Raz Blanchard is among the most promising tidal stream power sites. This section describes its general morphology and hydrodynamics.

C. Raz Blanchard morphology

The Raz Blanchard is situated in the Channel Sea, between La Hague cape in France and the Alderney Island. The tidal stream is concentrated in this 15 km wide passage. Its depth is well suited for tidal stream harvesting (around 50 metres depth).

The Raz Blanchard seabed morphology is complex (see Figure 2), as the seabed is composed of pebbles (0.2-0.5 metre diameter) and rocks. The relief is characterized by wave-cut platforms with 0.5-3 metres high rifts, canyons and small submarine hills.

The study zone of THYMOTE project is situated at the frontier between a deeper dune zone and a shallower rocky and rough zone. This choice allows studying different hydrodynamics conditions between ebb and flood. This site was selected for pre-commercial tidal farm testing (2015 French state call for projects).

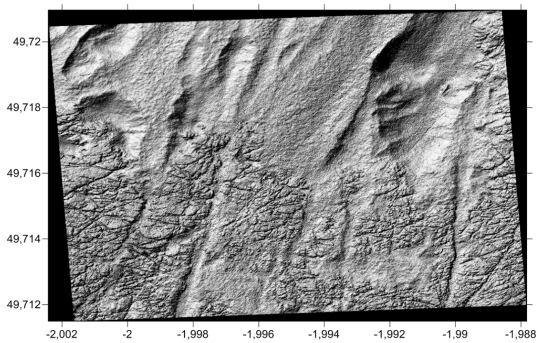

Fig. 2. The seabed morphology of the Raz Blanchard. Data from the French Naval Hydrographic and Oceanographic Service (SHOM).

D. Reference ADCP data

The reference for the numerical simulation comes from on-site measurements conducted in the framework of the THYMOTE project. Two coupled ADCP Teledyne RDI Workhorse Sentinel 600kHz were placed on the Raz Blanchard seabed (see Figure 3). The data are measured on 1.2 metres high cells, at a 2 Hz frequency, during 38 days between the September 27th and the November 3rd 2017. The data was treated to extract velocity [21] and velocity variance [22].

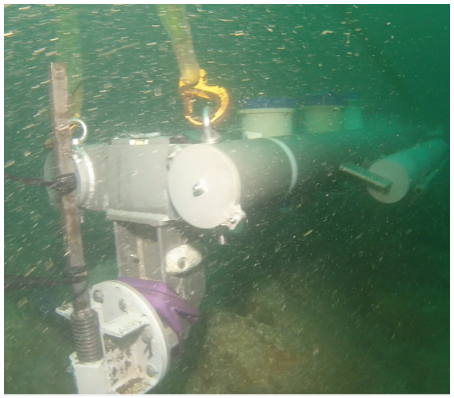

Fig. 3. THYMOTE ADCP on the Raz Blanchard seabed [23].

At the ADCP position, the tidal range varies between 1.5 metres the 29th of September 2017 (tidal coefficient 28) and 7 metres the 7th of October 2017 (tidal coefficient 104). The mean depth is 31.5 metres. The current direction relative to the north varies around 15° during flood and 197° during ebb. The maximum current magnitude varies between 2 $m.s^{-1}$ the September 29th 2017 and 5 $m.s^{-1}$ the October 7th 2017.

For the model validation, we opt for a period when the current magnitude and direction and the depth are stable. Figure 4 presents the time evolution of these three parameters during a flood tide. The conditions can be considered as stable over a 20 minute period, when the current magnitude is maximum.

IV. Simulation of a part of the Raz Blanchard

The objective of this work is the simulation, at a local scale, of Raz Blanchard tidal flow. It aims to understand and describe the physical phenomena responsible for the emission of turbulent vortices.

E. Simulation parameters

One big challenge of such a simulation is to generate proper inflow boundary conditions.
In particular, the distance required for the turbulence to develop over the whole water column is unknown. To restrict the size of the simulation domain, periodic boundary conditions are used in the longitudinal direction. A free slip boundary condition is applied on the water surface, and Dirichlet boundary conditions on the domain lateral sides. These boundary conditions are combined with an increase of viscosity near the boundaries to prevent numerical instabilities.

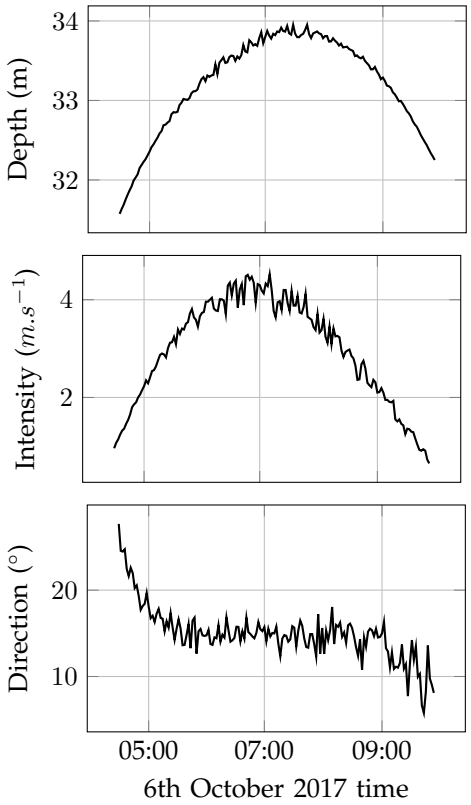

Fig. 4. Depth, current intensity and direction variations 20 metres above seabed, at ADCP location [23], for a 6 hour period.

The SHOM provides bathymetric data of the study zone with a spatial resolution of 1 metre. For the present purpose, a 300 mx80 m domain surrounding the ADCP has been selected to build the computational domain. We opt for simulating the peak flood conditions. The study zone has been oriented so that the longitudinal axis corresponds to current direction (15°/north). The ADCP is located near the outlet of the study zone, which is required to allow for a maximal turbulence development. As periodic boundary conditions are used, the selected zone has been enlarged on each side of the domain so that the water depth on the inlet corresponds to the water depth on the outlet. Those 10-metre long zones are visible on the top and the bottom of Figure 5.

The depth varies between 41 and 27 metres relatively to the lowest astronomical tide. A big asperity is situated in the middle of the domain. Several geologic cracks are visible in the domain (Figure 5). In this figure, the ADCP position is indicated by a black cross.

The mesh resolution ranges from 0.21 metres close to the seabed to 0.42 metres close to the surface. The time step is set to $6.25.10^{-3}$ seconds. The total number of nodes is 36.8 million. A volumetric force is used to sustain the flow. It is gradually fine-tuned until flow speed convergence. The final value corresponds to an acceleration of the flow of 2.10^{-3} $m.s^{-2}$.

Data acquisition starts after a stabilization period equivalent to 30 minutes of real-time. The data are extracted, at the location of the ADCP, during a 6 minute period. Data treatment provides time-averaged

profiles of velocity and velocity variance. The whole computation takes 30 hours on 112 processors.

The reference measurements correspond to a peak flood (October the 5th 2017 at 6:00 am). These data result for the treatment of 2 minute sample periods. Due to high variability of the results on successive sampling periods, the measurements data are averaged over 10 successive sampling periods (solid black curves in Figure 6), and the standard deviation relative to these 10 periods is plotted in dashed curves.

The coordinate system is based on the ADCP beam orientation. This avoids performing rotations on the variance tensor. The x axis is almost in the opposite direction of the flow (directed 109° from north), the y axis is almost perpendicular to the flow (directed 199° from north), and the z axis is vertical.

F. Results

Simulation results are compared to on-site measurements in Figure 6. The measured and simulated velocity profiles significantly differ. The longitudinal simulated speed fast tends to a stable value from the seabed to the surface, whereas the measured profile shows a much progressive evolution. The two other speed components agree well with measurements. The simulated variance profiles show a very low intensity in the highest part of the water column compared to measured data. However, the intensities of simulated variances are coherent with measurements near the seabed (distance smaller than 10 metres). This observation is verified for all six variance components. The influence of the water surface boundary condition is visible on uu, vv and ww components. It leads the turbulence intensity to zero at the water surface. However this influence seems to be confined to the firsts meters under the surface, and thus do not affect the comparison with measurement data.

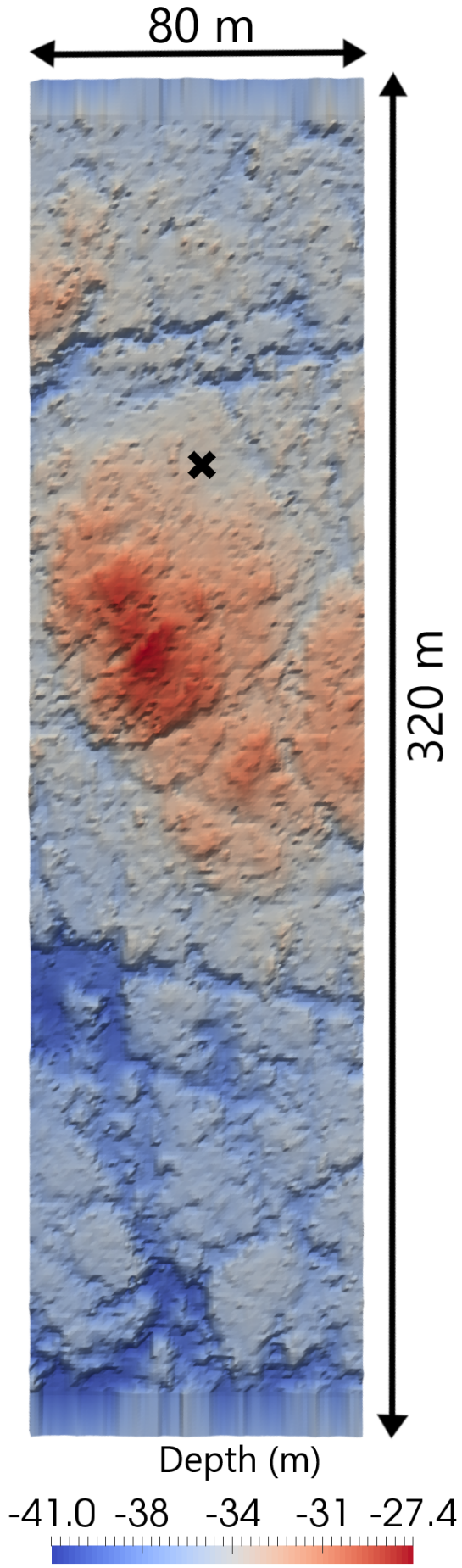

Fig. 5. Simulation domain (data from the SHOM). Top view.

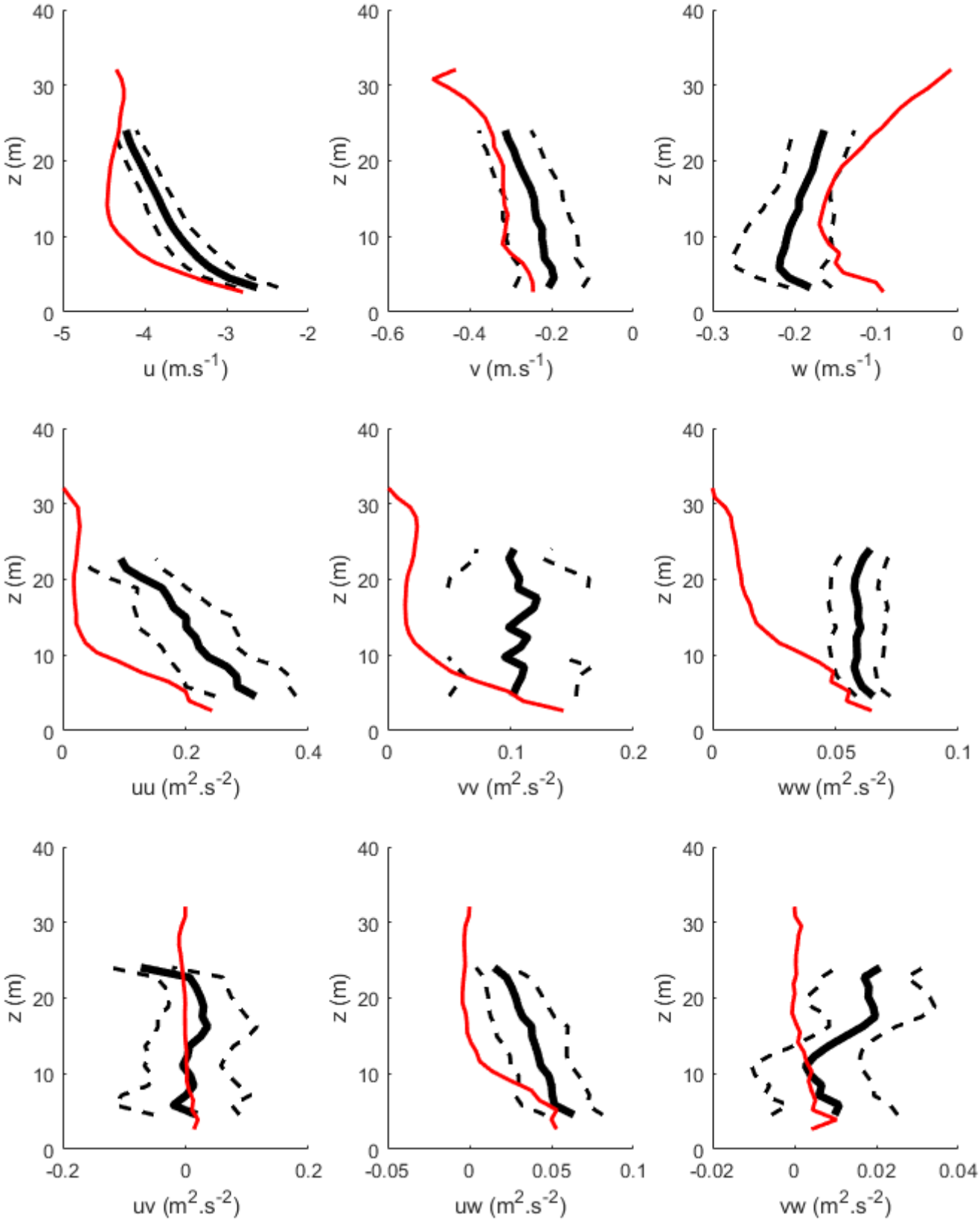

Fig. 6. Vertical profiles of velocity and velocity variance. In red: simulation results. In black: (solid) time average of measurements over a period of 20 minutes, (dashed) standard deviation of 2 minute samples relative to the 20 minute sample.

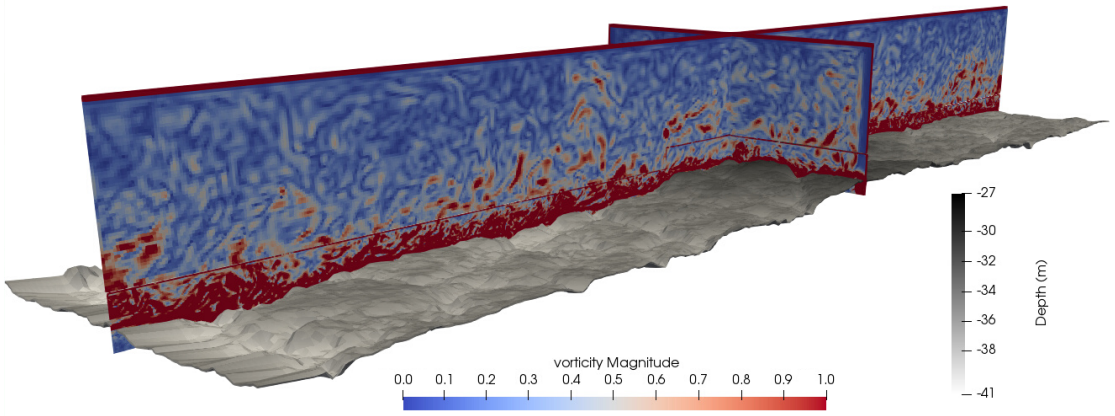

Fig. 7. Vorticity cuts in a simulated flow of a part of the Raz Blanchard.

The lack of turbulence intensity is also observed in Figure 7. Instantaneous vorticity along vertical planes show high vorticity in red and low vorticity in blue. Intense vortices are generated near the seabed. But most of them stay near the seabed and do not reach the surface.

However, large-scale turbulent vortices are generated in the simulation. A common hairpin vortex that took off from the seabed can be observed in Figure 8, which represents a lambda2 isosurface. As they develop in the flow, such vortices reach sizes around 20 metres.

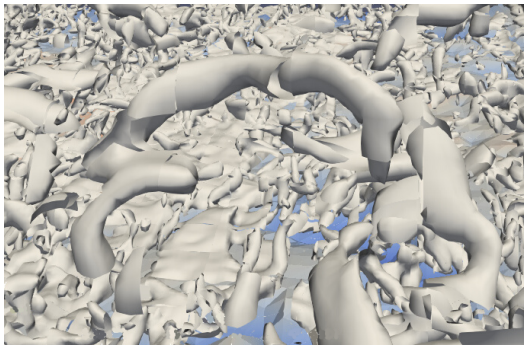

Fig. 8. LBM-LES simulated hairpin turbulent motion in a tidal power environmental flow. Lambda2 surface plot.

V. Conclusion

LES simulation of a Raz Blanchard tidal flow has been carried out. The simulation incorporated measured bathymetry and hydrodynamic parameters obtained from on-site measurements.

The simulation results are too far from the measurements to fully validate the simulation. Still, the speed variance is quite well reproduced close to the seabed. This suggests that the mesh resolution is not responsible for the poor results in the upper part of the water column. Indeed, the hydrodynamic conditions close to the seabed asperities are well reproduced. The hydrodynamic conditions in the upper part of the water column, more sensitive to the far upstream conditions, are thus missing, which may be due to a too short domain dimension in the longitudinal direction. Indeed, strong bathymetry variations are visible upstream the simulation domain, and may explain the high turbulence intensity of the high part of the water column.

Qualitative results are promising, with the detection of hazardous turbulent motions, which demonstrates the ability of the code to simulate these motions and paves the way to a better understanding of the link between seabed morphology and intense vortex emission.

The lattice Boltzmann method specificities make it a well-suited method to investigate local effect of the seabed morphology on turbulent events. Further work may allow to better understand the physics of environmental flows and to perform precise site characterization for the tidal stream power industry. Moreover, different boundary conditions at the water surface could be used to take into account the role of waves and wind on the turbulent characteristics of the flow near the surface.

References

[1] M. Lewis, S. P. Robins, and M. R. Hashemi, "Resource assessment for future generations of tidal-stream energy arrays," *Energy*, vol. 83, pp. 403–415, 2015. I

[2] T. A. A. Adcock, "The available power from tidal stream turbines in the pentland firth," *Proceedings of the Royal Society*, 2013. I

[3] V. T. Nguyen, S. S. Guillou, J. Thiébot, and A. S. Cruz, "Modelling turbulence with an actuator disk representing a tidal turbine," *Renewable Energy*, vol. 97, pp. 625–635, 2016. I

[4] D. S. Coles, L. S. Blunden, and A. S. Bahaj, "Assessment of the energy extraction potential at tidal sites around the channel islands," *Energy*, vol. 124, pp. 171–186, 2017. I

[5] O. A. L. Brutto, J. Thiébot, S. S. Guillou, and H. Gualous, "A semi-analytic method to optimize tidal farm layouts - application to the alderney race (raz blanchard), france," *Applied Energy*, vol. 183, pp. 1168–1180, 2016. I

[6] J. Thiébot, P. B. du Bois, and S. Guillou, "Numerical modeling of the effect of tidal stream turbines on the hydrodynamics and the sediment transport - application to the adlderney race (raz blanchard), france," *Renewable Energy*, vol. 75, pp. 356–365, 2015. I

[7] M. Togneri, M. Lewis, S. Neill, and I. Masters, "Comparison of adcp observations and 3d model simulations of turbulence at a tidal energy site," *Renewable Energy*, vol. 114, pp. 273–282, 2017. I

[8] T. Blackmore, W. M. J. Batten, and A. S. Bahaj, "Influence of turbulence on the wake of a marine current turbine simulator," *Proceedings of the Royal Society*, 2014. I

[9] T. Blackmore, L. E. Myers, and A. S. Bahaj, "Effects of turbulence on tidal turbines: Implications to perfomances, blade loads, and condition monitoring," *International Journal of Marine Energy*, vol. 14, pp. 1–26, 2016. I

[10] J. Thomson, B. Polagye, V. Durgesh, and M. Richmond, "Measurements of turbulence at two tidal energy sites in puget sound, wa," *IEEE Journal of oceanic engineering*, vol. 37, no. 3, 2012. I

[11] M. Thiébaut and A. Sentchev, "Tidal stream resource assessment in the dover strait (eastern english channel)," *International Journal of Marine Energy*, vol. 16, pp. 262–278, 2016. I

[12] M. Guerra, R. Cienfuegos, J. Thomson, and L. Suarez, "Tidal energy resource characterization in chacao channel, chile," *International Journal of Marine Energy*, vol. 20, pp. 1–16, 2017. I

[13] P. Sagaut, *Large Eddy Simulation for Incompressible Flows*. Scientific Computation, 2006. I, II

[14] Z. Guo and C. Shu, *Lattice Boltzmann Method and its applications in engineering*, W. Scientific, Ed. Advances in Computational Fluid Dynamics, 2013. I, II

[15] P. Mercier, M. Grondeau, S. Guillou, J. Thiébot, and E. Poizot, "Toward the modelling of turbulence at tidal stream power sites with the lattice boltzmann method," in *European Wave and Tidal Energy Conference*, 2017. I, II

[16] P. Bhatnagar, E. Gross, and M. Krook, "A model for collision processes in gases," *Physical Review*, vol. 94, no. 3, 1954. II

[17] J. Maxwell, "Illustrations of the dynamic theory of gases. part i. on the motions and collisions of perfectly elastic spheres." *Philosophical Magazine*, vol. 4, no. 19, pp. 19–32, 1860. II

[18] J. Latt and B. Chopard, "Lattice boltzmann method with regularized pre-collision distribution functions," *Mathematics and Computers in Simulation*, vol. 72, pp. 165–168, 2006. II

[19] J. Smagorinsky, "General circulation experiments with the primitive equations," *Monthly Weather Review*, vol. 91, no. 3, pp. 99–164, 1963. II

[20] C. Bailly and G. Comte-Bellot, *Turbulence*. CNRS Editions, 2003. II

[21] R. Dewey and S. Stringer, "Reynolds stresses and turbulent kinetic energy estimates from various adcp beam configurations: Theory," *Journal of Physical Oceanography*, pp. 1–35, December 2007. III

[22] B. Vermeulen, A. Hoitink, and M. Sassi, "Coupled adcps can yield complete reynolds stress tensor profiles in geophysical surface flows," *Geophysical Research Letters*, vol. 38, no. L06406, 2011. III

[23] N. Chaplain, T. Garlan, R. Duarte, and V. Barale, "L5.6/l5.7 rapport de campagne - campagne de mesures dans le raz blanchard." 3, 4